ACS Partner Journal

CHEMICAL & BIOMEDICAL IMAGING

pubs.acs.org/ChemBioImaging

Article

Long-Term Real-Time Tracking of Morphology and Migration of Neuronal Cells under Oxidative Stress

Ming-Kang Li, Ru-Jia Yu,* Ke-Le Chen, Yan Zhao, Cheng Yang,* Yong-Jing Wan, Yi-Tao Long, and Yi-Lun Ying

Cite This: *Chem. Biomed. Imaging* 2025, 3, 191−198

Read Online

ACCESS | Metrics & More | Article Recommendations | Supporting Information

ABSTRACT: Neuronal cells exhibit diverse morphologies that are crucial for their function within the neuronal network. Long-term quantitative analysis of both neuronal cell morphology and migration is essential in neuroscience research but remains challenging. Sodium arsenite, a known inducer of oxidative stress in neurons, affects both cell morphology and migration. To rapidly assess oxidative stress in HT22 neuronal cells, we developed a method for tracking key morphological features and migration trajectories of the individual cells. Three time-dependent parameters—velocity, circularity increment, and turn angle—are identified as rapid, direct indicators of the early stages of oxidative stress in neuronal cells. This method is then applied to investigate the effects of arsenite exposure on neuronal cells. Our approach provides a valuable tool for the rapid, label-free, and long-term real-time tracking of oxidative stress in neuronal cells, offering potential insights into cellular responses under stress conditions.

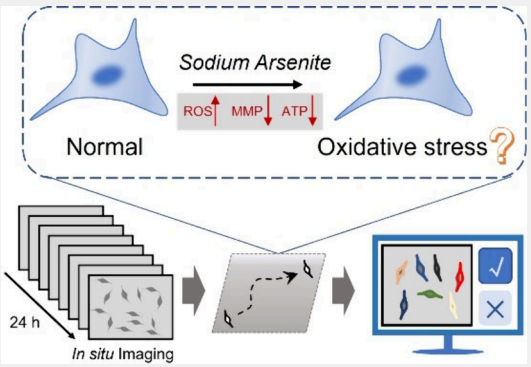

KEYWORDS: *Sodium arsenite, Oxidative stress, Real-time imaging, Cell morphology, Cell migration*

INTRODUCTION

Arsenite is a well-known human-caused environmental contaminant. Chronic arsenite exposure can cause skin diseases, cardiovascular diseases, and malignant tumors.[1] Notably, arsenite can readily cross the blood-brain barrier and cause neurological impairment.[2] Its neurotoxicity mechanism is highly associated with the induced oxidative stress in the nervous system, which at the molecular level includes the formation of stress granules,[3,4] and most visually manifests itself in corresponding changes in the morphology and migration of various types of neurons.[5,6] Cell migration is widely recognized as a fundamental biological process that occurs during embryonic development, playing a vital role not only in tissue building and maintenance but also in its repair and regeneration.[7−10] Specifically for individual cells, migration is associated with dynamic changes in cell morphology, which establish distinct biochemical front and rear regions, directing specific locomotion.[11−13] Among these motile cells, neurons typically display diverse morphologies, and some of their migration covers relatively long distances, with changes in direction within brain tissue.[14,15] Oxidative stress affects a variety of migration-related pathways and induces mitochondrial dysfunction, resulting in the inability of neuronal cells to maintain normal morphology and migration.[16−18] Arsenite-induced neurodevelopmental disorders and nerve damage are related to abnormal migration, yet there is a limited understanding of how neuron migration changes under arsenite exposure on the single-cell level.

Cellular morphology and migration are highly related to their biological functions in different microenvironments;[19] e.g., microglia convert into M1 or M2 types when confronted with pathogenic microorganisms,[20] and astrocytes exhibit two morphologically distinct phenotypes, A1 and A2, under different conditions.[21,22] In a typical neuron migration cycle, several integrated steps are involved, including leading-edge extension with distinct cellular polarization, migration of the cell body, and the retraction of the trailing process.[23] The periodic morphological changes during migration can directly affect the distance and direction.[24] Morphological differences between cells can distinguish the cell state changes and reflect the microenvironment in which they are located.[25] Therefore, it is of vital significance to quantitatively analyze the neuron morphology over time. A common method of cell morphology analysis involves collecting a large number of images by time-lapse live cell imaging microscopy and then acquiring cell shape parameters such as cell area and aspect ratio.[26−29]

Received: September 25, 2024
Revised: November 5, 2024
Accepted: November 8, 2024
Published: November 19, 2024

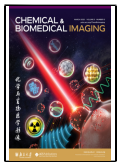

https://doi.org/10.1021/cbmi.4c00074
Chem. Biomed. Imaging 2025, 3, 191−198

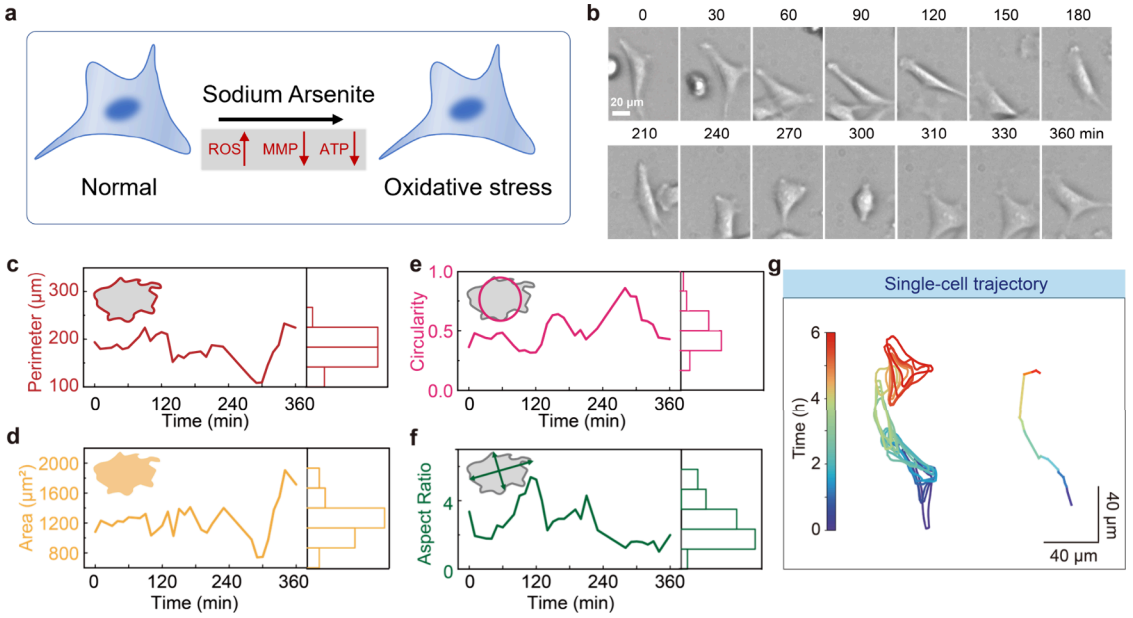

Figure 1. (a) Sodium-arsenite-induced oxidative stress affects neuronal cell morphology. (b) Time-lapse images of a representative HT22 cell during 360 min of recording in 30 min intervals. Considering the rapid morphology change at 300 min, the recording image at 310 min was supplied. (c–f) Time-series morphological characteristics (left panels) and the histograms (right panels) of the selected cell, showing cell perimeter (c), area (d), circularity (e), and aspect ratio (f). (g) Trajectories of the representative cell over 360 min, described by cell shapes (left) and cell centroids (right), respectively.

Although this method has advanced the study of tumor cells and keratinocytes, it remains challenging for neuronal cells due to their slow migration activity and complex morphological characteristics, which require imaging and statistics of a larger number of cells over prolonged periods. Manual analysis is time-consuming and error-prone, especially for the long-term tracking of large numbers of cells. A rapid analytical approach is needed to obtain the exact morphology and relative position of neuronal cells to monitor the effects of oxidative stress on neuronal cell migration.

In this study, we introduced a multiparametric cell morphology analysis strategy to assess oxidative stress in neurons (Figure 1a). By comparing the effects of oxidative stress at both the bulk and single-cell levels, we observed that arsenite-induced oxidative stress had a limited impact on static neuronal shape parameters such as cell area and circularity. However, time-dependent parameters—specifically, velocity, circularity increment, and turn angle—revealed a significant reduction in the frequency of neuronal morphology changes and changes in cellular motility patterns, ultimately leading to impaired migration. A self-developed multitarget tracking algorithm was employed for the morphology and migration analyses, which is capable of accurately identifying cells with complex morphology and tracking them over long periods of time.[30] Our findings emphasize the importance of time-dependent parameters in capturing dynamic morphological changes that occur in conjunction with cellular rotation and migration behaviors. Therefore, this approach is suitable for studying slowly migrating neuronal cells and facilitates the identification of oxidative stress in the cells.

RESULTS AND DISCUSSION

Long-Term Real-Time Tracking of Cell Morphology and Migration

In situ imaging of neuronal cells was performed via a live-cell dynamic imaging system, which enabled a long-term collection of time-lapse images within the incubator. Active migration as well as periodic morphological changes were observed in the cultured HT22 cells. Figure 1b shows the representative time-series morphologies in a typical HT22 cell over 360 min (the raw images are shown in Figure S1). It suggested that the cell underwent highly polarized morphologies and kept moving by extending a protrusion that migrated in a particular direction. Comparing the images recorded at 0 and 120 min, the extended protrusion prompted the cell to rapidly migrate toward the upper left of the field of view. The cell area shrunk to a circular shape after completing a period of migration, as shown in the recording time of 270 and 300 min. To quantify cell morphological change during migration, the algorithm mentioned above was used to identify and track the migrating cells (see Figure S2 for the original cellular identification). The morphology of neuronal cells was quantitively characterized using standard parameters including perimeter, area, circularity, and aspect ratio. Among these, perimeter and area represent, respectively, the contour and the surface enclosed by the cell membrane. Circularity and aspect ratio describe the roundness and polarity of a cell, with circular cells possessing a value of 1.0 for both parameters. Figure 1c–f describe detailed time-series morphological changes in the representative cell, with corresponding histograms shown on the right panels. Figure 1g illustrates cell migrations over the recording time, which contains time-series cell profiles identified from the time-lapse images. Furthermore, we employed cell centroids to simplify and pinpoint cell positions, facilitating the mapping of the cell migration trajectory with detailed distances and directions. Thus, long-term real-time tracking and quantitative

https://doi.org/10.1021/cbmi.4c00074
Chem. Biomed. Imaging 2025, 3, 191–198

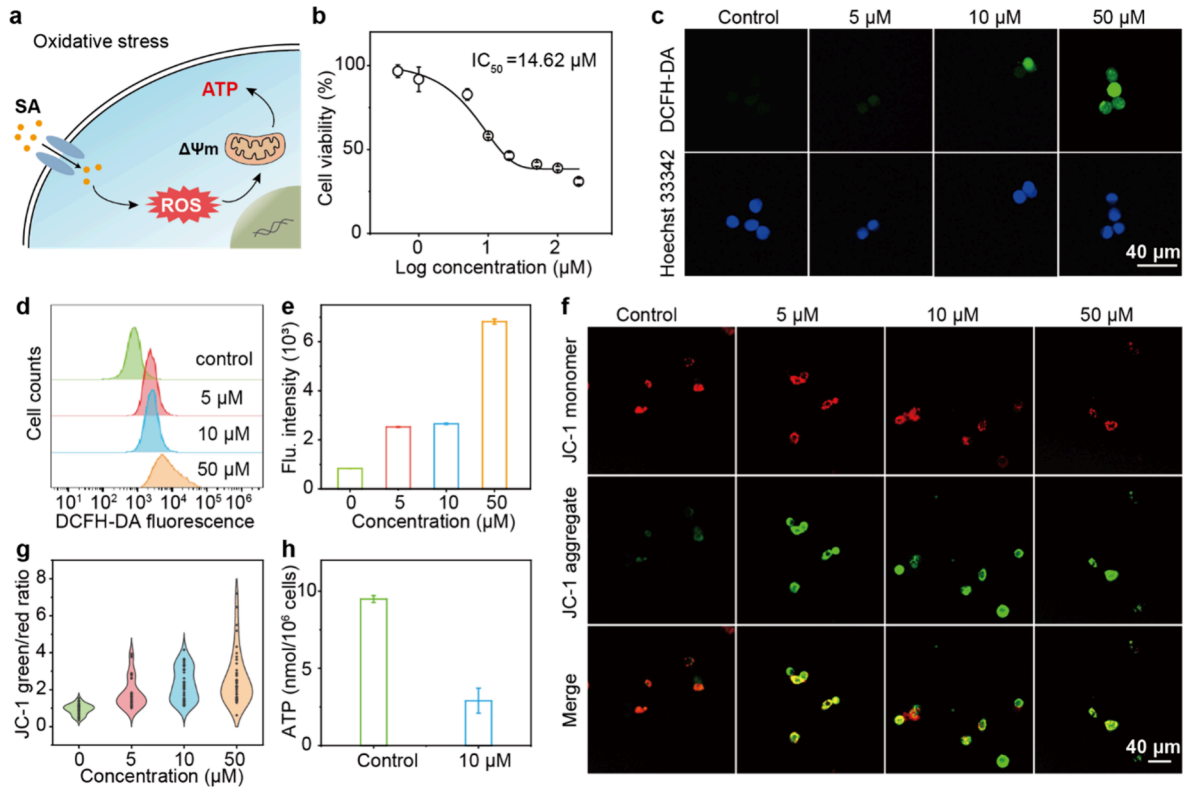

Figure 2. (a) Schematic illustration of oxidative stress in neuronal cells with SA treatment. (b) Cell viability of HT22 cells in response to increasing SA concentrations. CLSM images (c) and flow cytometry analysis (d) of the ROS in HT22 cells. (e) Quantitative analysis of ROS production by flow cytometry. (f) CLSM images of JC-1 fluorescence in HT22 cells. (g) Statistical fluorescence intensity of JC-1 green/red. (h) ATP levels in control and oxidatively stressed HT22 cells.

characterization of neuronal cell morphology and migration could be achieved using this method.

Throughout the 360 min recording, the perimeter and area remained relatively stable, while experiencing a sudden fluctuation between 240 and 330 min (Figure 1c,d). This fluctuation occurred exactly as the cell switched its migration direction by adjusting its shape. Comparatively, the characteristics of circularity and aspect ratio showed close relationships with active cell migration. As shown in Figure 1e,f, the periodic increase and decrease in the circularity and aspect ratio correlated well with the step motion of the cell. Typically, cell migration involves the extension or retraction of protrusions, which directly results in an obvious change in cell polarity. The cell exhibited a pair of protrusions to migrate in a specific direction, extending a third one to change its direction. During this period, a temporary contracted morphology was observed at 300 min, with the first two protrusions retracted and the third one not yet extended. At this point, the cell perimeter and area reached a minimum, with the circularity and aspect ratio approaching 1.0. These results suggested that cell perimeter and area, as the main intrinsic characteristics of cells, could be used as indicative of directional changes during cell migration. While circularity and aspect ratio are more suitable for reflecting the dynamic migration of cells. Overall, this method provides a fundamental correlation between cell morphology and migration, playing an important role in understanding the dynamic behavior of single cells during long-term recordings (~24 h).

Establishing a Neuronal Cell Model of Oxidative Stress

Sodium arsenite (SA) is well-known to induce oxidative stress in living cells and was used here to develop a neuronal cell model of oxidative stress (Figure 2a). Cytotoxicity on HT22 cells was first evaluated by exposing the cells to various concentrations of SA. As shown in Figure 2b, cell viability exhibited only a slight decrease at SA concentrations below 10 μM, whereas much reduction was observed at concentrations higher than 50 μM. It demonstrated that the survival rate dropped with elevated SA concentration from 97% at 0.5 μM to 21% at 500 μM. A median inhibition concentration (IC_{50}) of 14.62 μM was determined by using the DoseResp function fitting. Subsequently, SA concentrations of 5 μM and 10 μM with >50% viability were used to induce oxidative stress, while 50 μM was used as a control for apoptosis. The production of intracellular ROS was directly determined with the DCFH-DA probe, which could be oxidized into green fluorescent DCF in the presence of ROS. Cellular localization was performed by nuclear costaining using Hoechst 33342 (blue). The confocal laser scanning microscopy (CLSM) images in Figure 2c show that SA treatment resulted in a clear increase in the green fluorescence signal in HT22 cells. Further quantitative analysis with flow cytometry showed that intracellular ROS levels were produced in a SA concentration-dependent manner (Figure 2d,e). It is generally accepted that ROS production in oxidatively stressed cells leads to mitochondrial dysfunction, which includes both the depolarization of mitochondrial membrane potential (MMP) and impairment of mitochondrial activity. The cationic JC-1 dye was first utilized for specific mitochondrial labeling of neuronal cells, with a higher ratio of

https://doi.org/10.1021/cbmi.4c00074
Chem. Biomed. Imaging 2025, 3, 191−198

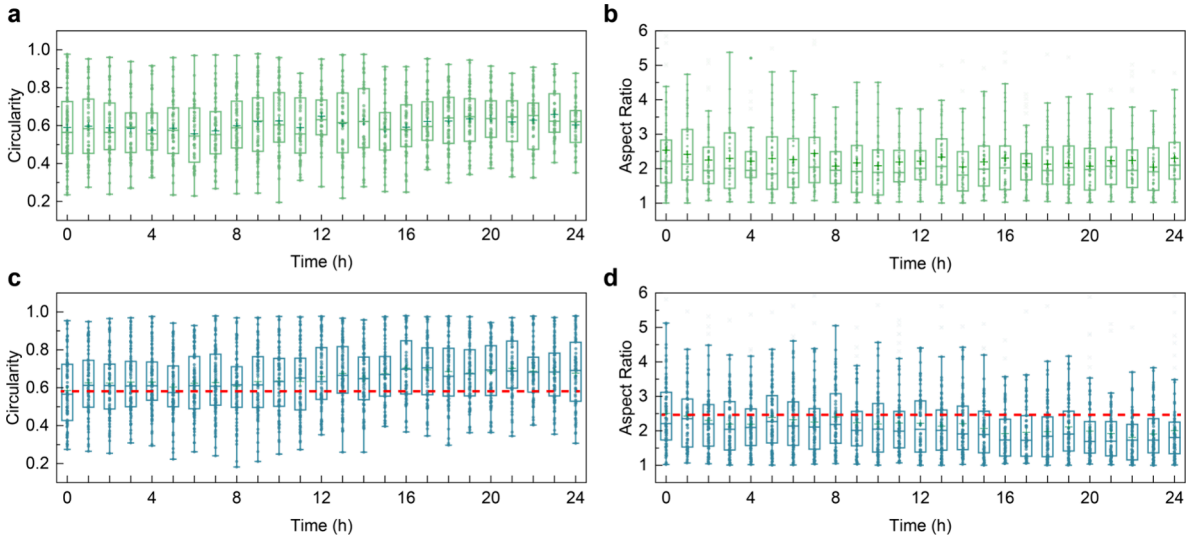

Figure 3. Cell circularity and aspect ratio were plotted over time-lapse acquisition duration, showing the normal neuronal cells (a,b) and oxidatively stressed cells (c,d) over 24 h. The number of cells in each figure is shown in Table S1. The red lines represent the mean value of circularity (c) and aspect ratio (d) when the cells were normal (0 h).

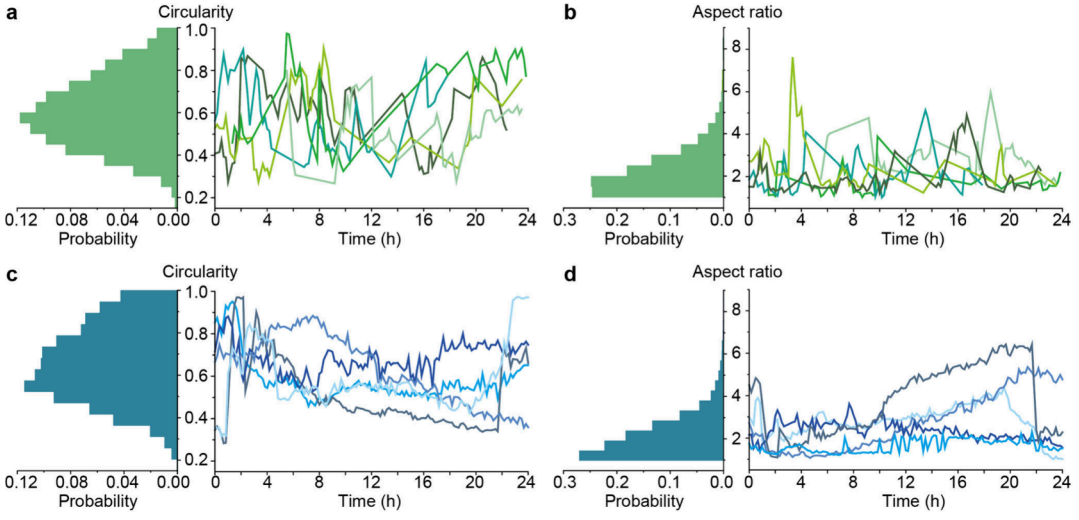

Figure 4. Cell morphology features of circularity (a) and aspect ratio (b) of the normal HT22 cells and circularity (c) and aspect ratio (d) of the oxidatively stressed HT22 cells. Left panels show the total collected features of the cells over 24 h (N = 7529 for a and b, N = 11 332 for c and d) and right panels show the corresponding time series features for five individual cells. The results from normal and oxidatively stressed cells are represented in green and blue, respectively.

green/red fluorescence (monomers/aggregates) revealing reduced MMP. As shown in the CLSM images in Figure 2f, distinct green-colored cells were observed in the SA-treated cells, whereas red-colored cells with JC-1 aggregates were observed in the control group. This clear depolarization of mitochondria revealed mitochondria dysfunction in the SA-treated HT22 cells. Statistical analysis in Figure 2g showed that the average green/red fluorescence ratio in the oxidatively stressed cells (treated with 10 μM SA) increased nearly 2-fold compared with the control, suggesting an MMP drop by almost two-thirds. Furthermore, the mitochondria activity of neuronal cells was evaluated by measuring the intracellular ATP level, which is also known to be commonly related to cell morphology and migratory events. Figure 2h shows that the ATP level in the oxidatively stressed cells reduced to one-third compared to the control, which corresponded well to the MMP drop. It was thus known that the oxidatively stressed neuronal cells, although the viability remained, exhibited obvious mitochondrial dysfunction, indicating that the SA treatment of HT22 cells could be used as a neuronal cell model of oxidative stress. Further cell morphology and migration tracking were subsequently performed to assess the effects of oxidative stress.

Analysis of Cell Morphology in Oxidatively Stressed Cells

To evaluate the influence of oxidative stress on neuron morphologies, HT22 cells with and without SA treatment were monitored and imaged using the proposed long-term tracking method. A large number of cells within the field of view were first identified using self-developed software. Bulk analysis and evaluation of the cellular morphology were implemented by including statistical morphological features over the recording time. There was little difference in either cell perimeter or area between the oxidatively stressed cells and the control (Figure S3), indicating that these two features were more likely to be

https://doi.org/10.1021/cbmi.4c00074
Chem. Biomed. Imaging 2025, 3, 191−198

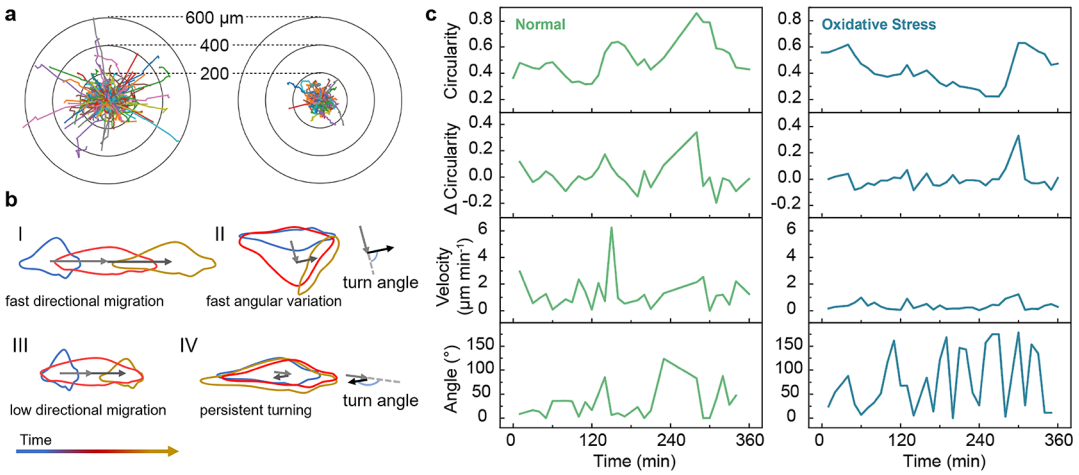

Figure 5. (a) Cell starting point normalized trajectories for neuronal cells in normal (left, N = 271) and oxidative stress (right, N = 207). (b) Schematic illustrations of the observed migration behaviors. (c) Time series of circularity, circularity increment, velocity, and turn angle in the control group (left) and oxidative stress (right panel).

intrinsic features of living cells. As mentioned before, cell viability remained in the oxidatively stressed cell but showed a high decrease in the mitochondrial activity and ATP level. To further evaluate whether this metabolic difference affects other morphological features, the population-averaged circularity and aspect ratio were plotted over time at 1-h intervals. As shown in Figure 3, the circularity of normal neuronal cells remained consistently around 0.6 during the 24-h recording (Figure 3a), and the aspect ratio was near 2 (Figure 3b). For the oxidatively stressed neuronal cells, there was a slight increase in the circularity observed after 12 h of recording (Figure 3c), correspondingly a slight decrease in the aspect ratio after 12 h (Figure 3d). Overall, the bulk analysis showed that oxidative stress in neuronal cells contributed minimally to the cell morphology, particularly during the early stages of stress (first 12 h). The apoptosis control of HT22 cells treated with 50 μM SA showed a clear decrease in cell perimeter, area, and aspect ratio as well as an increase in circularity, indicating that the cell morphology shrunk into a spherical shape from various polarized shapes (Figure S4).

Additionally, a single-cell analysis was performed by continuously tracking individual neuronal cells over time. Time-series analysis of single-cell circularity and aspect ratio exhibited a considerable difference between normal cells (Figure 4a,b) and oxidatively stressed cells (Figure 4c,d), although distributed similarly in statistical analysis of cell populations (shown in the left panel). Specifically, both the circularity and aspect ratio of normal cells showed large changes during the 24 h recording period, fluctuating rapidly and repeatedly in the ranges of 0.2−1.0 and 1−4, respectively. In contrast, oxidative stress in neuronal cells resulted in slower, smaller fluctuations in the ranges of these two features. Both circularity and aspect ratio showed obvious rapid changes during the first 6 h recording and then gradually became steady. Such time-series single-cell morphological characteristics could hardly be revealed by population distribution and can be uncovered through the time-series recording of individual cells. Consequently, the oxidative stress appeared to have a limited impact on cell morphology in statistical analysis; however, it reduced morphological changes at the single-cell level during long-term recording. This led us to focus on real-time tracking at the single-cell level by integrating individual cell morphological changes with migratory movements, which in turn will provide fundamental insights into the underlying mechanisms of oxidative stress in neuronal cells. To better reveal cell morphological features, we explored pairwise correlations among cell perimeter, area, circularity, and aspect ratio within a large population of neuronal cells. The correlation plot presented in Figure S5 indicated that circularity showed a stronger association with other morphological factors and thus was subsequently used for morphological characterization of migration in single-cell time-series analysis.

In-Depth Understanding of Single-Cell Morphology and Migration under Oxidative Stress

To describe the motility of individual cells during long-term monitoring, cell trajectories for both control and oxidative stress groups were plotted by using the center of mass for cell position. Figure 5a demonstrated a noticeable decrease in migration distance over 24 h, covering ∼200 μm in the control group and ∼100 μm in the oxidatively stressed cells. Additionally, there was a reduction in turning motility in the oxidatively stressed cells. Throughout the long-term recording, various migration behaviors were observed in these stochastic cell trajectories, with at least several general behaviors identified in Figure 5b, including fast directional migration with persistent polarization of the cell morphology (type I), fast angular variation with cellular polarization change (type II), low directional migration (type III), and persistent turning within a confined area (type IV).

To quantify the migration pattern of individual cells, as well as morphological behaviors during this period, three essential independent model parameters were utilized: circularity increment, velocity, and turn angle. These parameters were obtained from successive time-lapse images focusing on each cell. Among these, the circularity increment described the morphological changes of migrating cells, while velocity and turn angle indicated their migration patterns. Time-series representative migrating behaviors in 360 min were shown in Figure 5c for normal cells (left panel) and oxidatively stressed cells (right panel). As shown in the graphs, the representative cell in the control group exhibited two obvious circularity change behaviors at the time points ∼150 and 280 min, with two peak values of circularity and circularity increment. The

https://doi.org/10.1021/cbmi.4c00074
Chem. Biomed. Imaging 2025, 3, 191−198

former indicated a higher velocity and lower turn angle than the latter, corresponding to fast directional migration (type I) and fast angular variation (type II), respectively. Meanwhile, the cells in oxidative stress experienced relatively stable migrating behaviors with an overall velocity under 2 μm/min. The turn angle underwent rapid fluctuation during the recording, indicating that the cell migrated within a confined area, with the cell centroid moving randomly and leading to constant changes in the turn angle (type IV). Several proposed cell migration models have explained the migration of fibroblast cells or keratocytes, which highlighted the relationship between cell migration and actin.[26,31] Similarly, in this study, our results showed a transition from types I and II to types III and IV after oxidative stress. This observation suggests that long-term oxidative stress changes cell migration and reduces single-cell motility. The oxidative stress on the cells was also supported by the results from the MMP and intracellular ATP level (Figure 2). The effects of oxidative stress on actin and microfilament networks might be related to this transition.[32,33] The control group for cell apoptosis could be clearly revealed based on morphological features, with a rapid decrease in cell perimeter, area, and aspect ratio, as well as an increase in circularity. The overstressed cells shrank into a spherical shape and showed little migration (Figure S6).

The marked differences allow using their statistical results to create 3D scatter plots with 95% confidence of ellipsoids. Each dot depicts a single cell, and its corresponding parameters are acquired through a 2 h averaged value. Figure 6a shows that

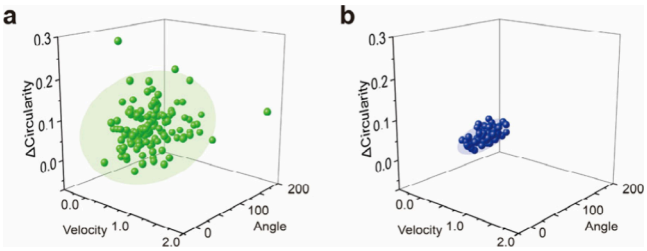

Figure 6. 3D scatter plot presenting the neuronal cells in the control group (a) and oxidative stress (b) with the axis of cellular velocity, turn angle, and circularity increment. Each dot represents a single cell. N = 113 for the normal cells; N = 149 for the oxidatively stressed cells.

the majority of the control neuronal cells were distributed in a more dispersed manner than the oxidatively stressed cell populations, yielding a centered velocity of 0.50 μm/min, a turn angle of 66°, and a circularity increment of 0.08. In contrast, the oxidatively stressed cell population in Figure 6b demonstrated a narrow distribution with a centered velocity of 0.23 μm/min, a centered turn angle of 88°, and a centered circularity increment of 0.04. Thus, our results showed that cell migration, together with the dynamic morphological variation, may be better for characterizing the early state of oxidative stress in neuronal cells. These morphological and migratory features of single cells could thus be utilized for the classification of cell populations and hold further potential for pathological applications. In addition, this method framework could also be applied to other cells including microglia and astrocytes, which have morphology changes under oxidative stress.[34,35]

CONCLUSIONS

In summary, the long-term morphology and migration of neuronal cells were characterized in detail in real time. In contrast to the detection of ROS by fluorescent probes, this method requires no labeling and could trace the effect of oxidative stress on the cells. It suggested that oxidative stress contributed less to cellular morphology based on statistical analysis, preserving various cellular morphologies at specific time points while reducing morphological changes in time-series single-cell analysis. This resulted in an obvious decrease in cell migration during long-term tracking. Specifically, multiple characteristic migration models were identified and described to illustrate the effect of oxidative stress on neuronal cells. It is known that cell migration is the result of the combined action of multiple proteins and molecules within the cell. Future advancements in molecular biology techniques offer the potential for an in-depth investigation in this field to explore the correlation between migration-related proteins and stress granules. Additionally, further identification of leader cells within a population would elucidate the cellular heterogeneity through biological relevance. In short, much could be expected through this proposed method for the long-term tracking of neuronal cells at both bulk and single-cell levels and the rapid detection of cells under oxidative stress.

ASSOCIATED CONTENT

Supporting Information

The Supporting Information is available free of charge at https://pubs.acs.org/doi/10.1021/cbmi.4c00074.

Experimental section, primary and algorithm-recognized cell pictures, correlation network, time-series morphological characteristics, and cell trajectories (PDF)

AUTHOR INFORMATION

Corresponding Authors

Ru-Jia Yu − *School of Chemistry and Chemical Engineering, Molecular Sensing and Imaging Center (MSIC), Nanjing University, Nanjing 210023, People's Republic of China;* orcid.org/0000-0002-5376-3648; Email: iamrjyu@njupt.edu.cn

Cheng Yang − *School of Electronic Sciences and Engineering, Nanjing University, Nanjing 210023, People's Republic of China*; Email: cyang@nju.edu.cn

Authors

Ming-Kang Li − *School of Chemistry and Chemical Engineering, Molecular Sensing and Imaging Center (MSIC), Nanjing University, Nanjing 210023, People's Republic of China*

Ke-Le Chen − *School of Chemistry and Chemical Engineering, Molecular Sensing and Imaging Center (MSIC), Nanjing University, Nanjing 210023, People's Republic of China*

Yan Zhao − *School of Information Science and Engineering, East China University of Science and Technology, Shanghai 200237, People's Republic of China*

Yong-Jing Wan − *School of Information Science and Engineering, East China University of Science and Technology, Shanghai 200237, People's Republic of China*

Yi-Tao Long − *School of Chemistry and Chemical Engineering, Molecular Sensing and Imaging Center (MSIC),*

Nanjing University, Nanjing 210023, People's Republic of China; orcid.org/0000-0003-2571-7457

Yi-Lun Ying − *School of Chemistry and Chemical Engineering, Molecular Sensing and Imaging Center (MSIC) and Chemistry and Biomedicine Innovation Center, Nanjing University, Nanjing 210023, People's Republic of China;* orcid.org/0000-0001-6217-256X

Complete contact information is available at: https://pubs.acs.org/10.1021/cbmi.4c00074

Notes

The authors declare no competing financial interest.

■ ACKNOWLEDGMENTS

This research was supported by the National Key Research and Development Program of China (2022YFA1205004), the National Natural Science Foundation of China (22276089), programs for high-level entrepreneurial and innovative talents introduction of Jiangsu Province, and Integrated Key Project of Ministry of Education - Top Talents Recruitment Program.

■ REFERENCES

(1) Lou, Q.; Zhang, M.; Zhang, K.; Liu, X.; Zhang, Z.; Zhang, X.; Yang, Y.; Gao, Y. Arsenic Exposure Elevated ROS Promotes Energy Metabolic Reprogramming with Enhanced AKT-Dependent HK2 Expression. *Sci. Total Environ.* **2022**, *836*, 155691.

(2) Wang, H.; Liu, X.; Chen, Y.; Li, W.; Ge, Y.; Liang, H.; Xu, B.; Li, X. The Regulatory Role of MiR-21 in Ferroptosis by Targeting FTH1 and the Contribution of Microglia-Derived MiR-21 in Exosomes to Arsenic-Induced Neuronal Ferroptosis. *J. Hazard. Mater.* **2024**, *478*, 135580.

(3) Hu, K.; Relton, E.; Locker, N.; Phan, N. T. N.; Ewing, A. G. Electrochemical Measurements Reveal Reactive Oxygen Species in Stress Granules. *Angew. Chem., Int. Ed.* **2021**, *60*, 15302−15306.

(4) Gu, H.; Gu, C.; Locker, N.; Ewing, A. G. Amperometry and Electron Microscopy Show Stress Granules Induce Homotypic Fusion of Catecholamine Vesicles. *Angew. Chem., Int. Ed.* **2024**, *63*, No. e202400422.

(5) Amuno, S.; Shekh, K.; Kodzhahinchev, V.; Niyogi, S. Neuropathological Changes in Wild Muskrats (Ondatra Zibethicus) and Red Squirrels (Tamiasciurus Hudsonicus) Breeding in Arsenic Endemic Areas of Yellowknife, Northwest Territories (Canada): Arsenic and Cadmium Accumulation in the Brain and Biomarkers of Oxidative Stress. *Sci. Total Environ.* **2020**, *704*, 135426.

(6) Singhal, A.; Morris, V. B.; Labhasetwar, V.; Ghorpade, A. Nanoparticle-Mediated Catalase Delivery Protects Human Neurons from Oxidative Stress. *Cell Death Dis.* **2013**, *4*, e903−e903.

(7) Ridley, A. J.; Schwartz, M. A.; Burridge, K.; Firtel, R. A.; Ginsberg, M. H.; Borisy, G.; Parsons, J. T.; Horwitz, A. R. Cell Migration: Integrating Signals from Front to Back. *Science* **2003**, *302*, 1704−1709.

(8) Mayor, R.; Etienne-Manneville, S. The Front and Rear of Collective Cell Migration. *Nat. Rev. Mol. Cell. Biol.* **2016**, *17*, 97−109.

(9) Cui, Y.; An, Y.; Jin, T.; Zhang, F.; He, P. Real-Time Monitoring of Skin Wound Healing on Nano-Grooves Topography Using Electric Cell-Substrate Impedance Sensing (ECIS). *Sens. Actuators B Chem.* **2017**, *250*, 461−468.

(10) Zhu, L.; Liu, H.-W.; Yang, Y.; Hu, X.-X.; Li, K.; Xu, S.; Li, J.-B.; Ke, G.; Zhang, X.-B. Near-Infrared Fluorescent Furin Probe for Revealing the Role of Furin in Cellular Carcinogenesis and Specific Cancer Imaging. *Anal. Chem.* **2019**, *91*, 9682−9689.

(11) Poduri, A.; Volpe, J. J. Chapter 6 - Neuronal Migration. In *Volpe's Neurology of the Newborn*, sixth ed.; Volpe, J. J., Inder, T. E., Darras, B. T., de Vries, L. S., du Plessis, A. J., Neil, J. J., Perlman, J. M., Eds.; Elsevier, 2018; pp 120−144.e8.

(12) Li, H.; Gao, J.; Cao, L.; Xie, X.; Fan, J.; Wang, H.; Wang, H.-H.; Nie, Z. A DNA Molecular Robot That Autonomously Walks on the Cell Membrane to Drive Cell Motility. *Angew. Chem., Int. Ed.* **2021**, *60*, 26087−26095.

(13) Liu, Y.; Wang, Y.-J.; Du, Y.; Liu, W.; Huang, X.; Fan, Z.; Lu, J.; Yi, R.; Xiang, X.-W.; Xia, X.; Gu, H.; Liu, Y.-J.; Liu, B. DNA Nanomachines Reveal an Adaptive Energy Mode in Confinement-Induced Amoeboid Migration Powered by Polarized Mitochondrial Distribution. *Proc. Natl. Acad. Sci. U. S. A.* **2024**, *121*, No. e2317492121.

(14) Sun, G. J.; Zhou, Y.; Stadel, R. P.; Moss, J.; Yong, J. H. A.; Ito, S.; Kawasaki, N. K.; Phan, A. T.; Oh, J. H.; Modak, N.; Reed, R. R.; Toni, N.; Song, H.; Ming, G. Tangential Migration of Neuronal Precursors of Glutamatergic Neurons in the Adult Mammalian Brain. *Proc. Natl. Acad. Sci. U. S. A.* **2015**, *112*, 9484−9489.

(15) Allen, G. M.; Lee, K. C.; Barnhart, E. L.; Tsuchida, M. A.; Wilson, C. A.; Gutierrez, E.; Groisman, A.; Theriot, J. A.; Mogilner, A. Cell Mechanics at the Rear Act to Steer the Direction of Cell Migration. *Cell Syst.* **2020**, *11*, 286−299.

(16) Liu, X.; Wang, F.; Fan, X.; Chen, M.; Xu, X.; Xu, Q.; Zhu, H.; Xu, A.; Pouladi, M. A.; Xu, X. CHCHD2 Up-Regulation in Huntington Disease Mediates a Compensatory Protective Response against Oxidative Stress. *Cell Death Dis.* **2024**, *15*, 126.

(17) Hara, T.; Toyoshima, M.; Hisano, Y.; Balan, S.; Iwayama, Y.; Aono, H.; Futamura, Y.; Osada, H.; Owada, Y.; Yoshikawa, T. Glyoxalase I Disruption and External Carbonyl Stress Impair Mitochondrial Function in Human Induced Pluripotent Stem Cells and Derived Neurons. *Transl. Psychiatry* **2021**, *11*, 275.

(18) Behar, T. N.; Colton, C. A. Redox Regulation of Neuronal Migration in a down Syndrome Model. *Free Radic. Biol. Med.* **2003**, *35*, 566−575.

(19) Liu, X.; Chi, W.; Qiao, Q.; Kokate, S. V.; Cabrera, E. P.; Xu, Z.; Liu, X.; Chang, Y.-T. Molecular Mechanism of Viscosity Sensitivity in BODIPY Rotors and Application to Motion-Based Fluorescent Sensors. *ACS Sens.* **2020**, *5*, 731−739.

(20) Feng, L.; Dou, C.; Xia, Y.; Li, B.; Zhao, M.; Yu, P.; Zheng, Y.; El-Toni, A. M.; Atta, N. F.; Galal, A.; Cheng, Y.; Cai, X.; Wang, Y.; Zhang, F. Neutrophil-like Cell-Membrane-Coated Nanozyme Therapy for Ischemic Brain Damage and Long-Term Neurological Functional Recovery. *ACS Nano* **2021**, *15*, 2263−2280.

(21) Stöberl, N.; Maguire, E.; Salis, E.; Shaw, B.; Hall-Roberts, H. Human IPSC-Derived Glia Models for the Study of Neuroinflammation. *J. Neuroinflammation* **2023**, *20*, 231.

(22) Zeng, Y.-L.; Du, Y.; Xu, X.-X.; Wang, Y.-J.; Yu, S.-X.; Liu, T.; Luo, S.; Xiang, X.-W.; Liu, W.; Chen, Y.-C.; Huang, H.; Gao, H.; Shen, Y.; Luo, Y.; Bao, C.; Liu, Y.-J. On-Chip Modeling of Physiological and Pathological Blood-Brain Barrier Microenvironment for Studying Glial Responses to Neuroinflammation. *Nano Today* **2023**, *52*, 101947.

(23) Bodor, D. L.; Pönisch, W.; Endres, R. G.; Paluch, E. K. Of Cell Shapes and Motion: The Physical Basis of Animal Cell Migration. *Dev. Cell* **2020**, *52*, 550−562.

(24) Ayala, R.; Shu, T.; Tsai, L.-H. Trekking across the Brain: The Journey of Neuronal Migration. *Cell* **2007**, *128*, 29−43.

(25) Wertheim, L.; Edri, R.; Goldshmit, Y.; Kagan, T.; Noor, N.; Ruban, A.; Shapira, A.; Gat-Viks, I.; Assaf, Y.; Dvir, T. Regenerating the Injured Spinal Cord at the Chronic Phase by Engineered IPSCs-Derived 3D Neuronal Networks. *Adv. Sci.* **2022**, *9*, 2105694.

(26) Keren, K.; Pincus, Z.; Allen, G. M.; Barnhart, E. L.; Marriott, G.; Mogilner, A.; Theriot, J. A. Mechanism of Shape Determination in Motile Cells. *Nature* **2008**, *453*, 475−480.

(27) Zhou, M.; Ma, Y.; Chiang, C.-C.; Rock, E. C.; Luker, K. E.; Luker, G. D.; Chen, Y.-C. High-Throughput Cellular Heterogeneity Analysis in Cell Migration at the Single-Cell Level. *Small* **2023**, *19*, 2206754.

(28) Mohammed, D.; Charras, G.; Vercruysse, E.; Versaevel, M.; Lantoine, J.; Alaimo, L.; Bruyère, C.; Luciano, M.; Glinel, K.; Delhaye, G.; Théodoly, O.; Gabriele, S. Substrate Area Confinement Is a Key

Determinant of Cell Velocity in Collective Migration. *Nat. Phys.* **2019**, *15*, 858−866.
(29) Masuzzo, P.; Van Troys, M.; Ampe, C.; Martens, L. Taking Aim at Moving Targets in Computational Cell Migration. *Trends Cell Biol.* **2016**, *26*, 88−110.
(30) Zhao, Y.; Chen, K.-L.; Shen, X.-Y.; Li, M.-K.; Wan, Y.-J.; Yang, C.; Yu, R.-J.; Long, Y.-T.; Yan, F.; Ying, Y.-L. HFM-Tracker: A Cell Tracking Algorithm Based on Hybrid Feature Matching. *Analyst* **2024**, *149*, 2629−2636.
(31) Ebata, H.; Yamamoto, A.; Tsuji, Y.; Sasaki, S.; Moriyama, K.; Kuboki, T.; Kidoaki, S. Persistent Random Deformation Model of Cells Crawling on a Gel Surface. *Sci. Rep.* **2018**, *8*, 5153.
(32) Huot, J.; Houle, F.; Marceau, F.; Landry, J. Oxidative Stress-Induced Actin Reorganization Mediated by the P38 Mitogen-Activated Protein Kinase/Heat Shock Protein 27 Pathway in Vascular Endothelial Cells. *Circ. Res.* **1997**, *80*, 383−392.
(33) Huot, J.; Houle, F.; Spitz, D. R.; Landry, J. HSP27 Phosphorylation-Mediated Resistance against Actin Fragmentation and Cell Death Induced by Oxidative Stress1. *Cancer. Res.* **1996**, *56*, 273−279.
(34) Qin, L.; Liu, Y.; Hong, J.-S.; Crews, F. T. NADPH Oxidase and Aging Drive Microglial Activation, Oxidative Stress, and Dopaminergic Neurodegeneration Following Systemic LPS Administration. *Glia* **2013**, *61*, 855−868.
(35) Chen, Y.; Qin, C.; Huang, J.; Tang, X.; Liu, C.; Huang, K.; Xu, J.; Guo, G.; Tong, A.; Zhou, L. The Role of Astrocytes in Oxidative Stress of Central Nervous System: A Mixed Blessing. *Cell Prolif.* **2020**, *53*, No. e12781.

https://doi.org/10.1021/cbmi.4c00074
Chem. Biomed. Imaging 2025, 3, 191−198